ELSEVIER

Journal of Crystal Growth 233 (2001) 868–880

JOURNAL OF CRYSTAL GROWTH

www.elsevier.com/locate/jcrysgro

Recrystallization phenomena of solution grown paraffin dendrites

F.F.A. Hollander[a], O. Stasse[a], J. van Suchtelen[a,b], W.J.P. van Enckevort[a,*]

[a] *RIM Laboratory, Department of Solid State Chemistry, Faculty of Science, University of Nijmegen, Toernooiveld 1, 6525 ED Nijmegen, Netherlands*

[b] *MESA Research Institute, University of Twente, P.O. Box 217, 7500 AE Enschede, The Netherlands*

Received 1 December 2000; accepted 29 June 2001
Communicated by M.E. Glicksman

Abstract

Paraffin crystals were grown from decane solutions using a micro-Bridgman set up for in-situ observation of the morphology at the growth front. It is shown that for large imposed velocities, dendrites are obtained. After dendritic growth, aging or recrystallization processes set in rather quickly, changing the crystal shapes considerably from the well-known dendritic shapes of melt grown dendrites. It is shown that several factors may cause these post-growth shape transitions: surface minimization, uptake and subsequent sweating of solvent material, and polymorphic phase conversion. It is shown that the first two recrystallization mechanisms are the most important for tricosane (n-$C_{23}H_{48}$) and pentacosane (n-$C_{25}H_{52}$) dendrites. Surface minimization by increasing the thickness of the crystals is particularly favorable. For dotriacontane (n-$C_{32}H_{66}$) dendrites, the recrystallization behavior appears to be less dramatic. It is shown that the uptake and sweating out of solvent material afterwards may lead to formation of holes within the dendrites.

PACS: 81.10.; 81.30.F; 64.70.K

Keywords: A1. Crystal morphology; A1. Dendrites; A1. Directional solidification; A1. Optical microscopy; A1. Recrystallization; B1. Organic compounds

1. Introduction

1.1. Dendrite growth and post-growth recrystallization

Recently, many efforts have been invested in a fundamental understanding of the solidification of materials. Morphologically unstable patterns, like dendritic or seaweed like crystals [1,2] have attracted much theoretical interest. Most studies assume that the dendrites are grown from the melt and have microscopically rough faces. Dendritic growth experiments that fulfill these assumptions are now well-understood. Anisotropy in the surface tension is necessary for obtaining dendrites, as dendrites reflect their underlying crystallographic lattice. If the crystal lacks an anisotropic surface tension, seaweed crystals are obtained [2,3] that do

*Corresponding author. Tel.: +31-24-365-3433; fax: +31-24-365-3067.

E-mail address: wvenck@sci.kun.nl (W.J.P. van Enckevort).

0022-0248/01/$ - see front matter
PII: S0022-0248(01)01602-5

not exhibit the regular-branched structure of dendrites. Both dendritic and seaweed patterns can be compact or fractal-like depending on the applied supercooling [2].

For dendritic patterns grown from solution, the theories developed for melt grown patterns may be applied [4]. The main differences involve different definitions of the important quantities determining the problem, such as the dimensionless diffusion field and the effective supersaturation. One important difference emphasized here is that for solution growth, the transport-limiting factor is the diffusion of growth units towards the interface, instead of the transport of generated latent heat away from the interface in the solidification processes.

All studies concerning dendritic growth mentioned above paid a lot of attention to the actual shape of the growth front of dendritic crystals. However, the post-growth recrystallization phenomena received less attention. The most important recrystallization process in solidification from the melt is the formation and recrystallization of grain boundaries, which can be studied by phase field modeling [5]. For solution growth, the reduction of the excess of surface generated during the growth process also drives the recrystallization processes, but grain formation is less important and recrystallization manifests itself in a different way. A well-known example, already shown by Saratovkin in the 1950s [6] is the recrystallization effect after dendritic growth of ammonium chloride, grown from an aqueous solution. Directly after the formation of the dendrites, arms are pinched off and develop into elongated single crystals. Several hours after growth, the entire pattern is changed into a macroscopic dendrite consisting of numerous elongated single crystals. Bienfait [7] showed that if ammonium chloride dendrites are grown in small, isolated, droplets with a radius less than a millimeter, the initially grown dendrites transform into a facetted crystal, within 100 h. This example shows that the time scale of recrystallization can be extremely important for the final material properties of solution grown crystals. In this chapter, we will show the possible effects of the surface minimization and the uptake of solvent material on the final shape of Bridgman grown paraffin dendrites from decane solutions.

1.2. Paraffins

Long chain compounds, such as n-alkanes and fats show a rich phase diagram of different polymorphs [8]. For n-alkanes up to approximately 44 carbon atoms, four main polymorphs are important depending on the number of carbon atoms, the purity and the applied supersaturation. These four polymorphs are "rotator", monoclinic, triclinic and orthorhombic. The rotator phase, which is normally detected just below the freezing point, is a special phase, showing characteristics of both liquids and crystalline solids [9,10] and are therefore considered as plastic crystals. This phase has the three-dimensional long-range order of the molecules, but lacks the long-range order in the rotational degree of freedom of the molecule about its long axis. Hence these crystals are isotropic in the plane perpendicular to the long axes of the molecules, implying that the morphology of such crystals must be disc-shaped, as shown by Van Hoof for tricosane [11]. Succinonitrile (SCN, $NC(CH_2)_2CN$) and camphene [12] are other examples of plastic crystals, always showing dendritic crystals that resemble the shape predicted by the solidification theories mentioned above, although not in a quasi two-dimensional shape like paraffins.

Besides the rotator phase, which is stable just below the melting temperature, all paraffins have a low-temperature ordered state, which, depending on the number of carbon atoms and purity, may be triclinic, orthorhombic or monoclinic polymorphs. In this study we will only focus on tricosane (n-$C_{23}H_{48}$), pentacosane (n-$C_{25}H_{52}$) and dotriacontane (n-$C_{32}H_{66}$) crystals, for which the orthorhombic polymorph is the most stable one.

The morphology of paraffin crystals is platelet-like, showing large top and bottom {0 0 1} faces. Except for the rotator phase, the side faces of the crystals are facetted, when grown at low supersaturation and moderate temperatures. The effect of the various polymorphic forms on the morphology of paraffins is not as large as the effect of chain length of the paraffin itself. In general, the longer

the chain, the thinner the crystal will be [13]. The thickness of paraffin crystals is very important for recrystallization effects. Van Hoof et al. [14] showed that at low supersaturation, during the same experiment, thin orthorhombic tricosane crystals dissolve, whereas thicker crystals grow within close vicinity. Using Monte-Carlo simulations, they showed that due to the Gibbs–Thomson effect, the curvature of the side faces is too large for the thin crystals, resulting in their dissolution.

2. Experimental procedure

For sample preparation, tricosane (n-$C_{23}H_{46}$), pentacosane (n-$C_{25}H_{52}$) or dotriacontane (n-$C_{32}H_{66}$) is dissolved in decane at approximately 50°C, with mass fractions of 0.4–0.75. All chemicals were purchased from Sigma-Aldrich and have 99% purity. One small droplet of solution is placed on an ordinary microscope preparation glass of 2 mm thickness and is covered by a thin cover glass of 0.17 mm thickness. Pressing gently onto the cover glass squeezes out the excess of material. With this technique, the thickness of the resulting film is less then 10 μm. The sample is then placed in the micro-Bridgman furnace as depicted in Fig. 1. The temperature of the hot finger is generated using an electrical heating wire and allows temperatures up to 300°C. The cold finger is constructed by using a water flow of constant temperature, generated by a thermostatic bath. The distance d between both fingers can be adjusted between 1 and 5 cm, but 1.5 cm is used in all experiments. Between the fingers, the growth front can be observed using a microscope equipped with a digital camera or video. The sample and sample holder can be translated at different speeds using a stepping motor. After starting the experiment, the system is assumed to be in a steady state when the growth front remains at a fixed position with respect to coordination frame of the microscope.

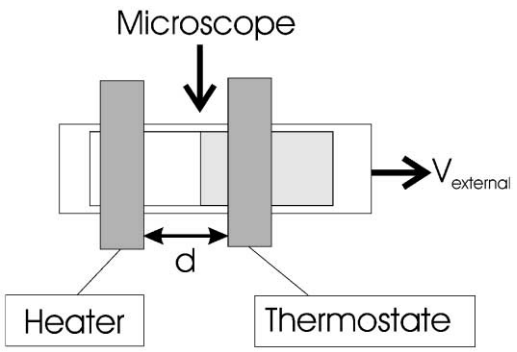

Fig. 1. The in situ Bridgman furnace. The thermostatic bath and heater regulate the temperatures of the cold and hot finger, respectively. The stepping motor with a pulling velocity $V_{external}$ translates the sample.

Polarizers, which are slightly misaligned from "crossed orientation", are used to obtain images with the highest contrast. In most cases, this is the only way to observe the thin dendrites at the growth-front. Unfortunately, the growing crystals are not birefringent, so no quantitative information on crystal thickness can be obtained by using the method described in our earlier work on paraffin growth [14,15]. However, comparing the image contrasts of the dendrite tips with that found in these in-situ studies indicates that the crystal thickness is in the order of one micrometer or somewhat less. This is confirmed by the occurrence of several overlapping dendrites within the 10 μm thick cell as observed during some experiments. From the difference in image contrast when two dendrites of similar thickness overlap, an idea of the contrast change as a function of crystal thickness is obtained. Since the crystals appearing at the growth front are not birefringent this supports our assumption that these crystals are grown in the rotator phase. Moreover, birefringent paraffin crystals, indicating an orthorhombic polymorph, are only observed after the experiment. This suggests that the solid state transition from the rotator to the orthorhombic state takes place after growth. The transition is normally not observed during the experiments, except for highly concentrated solutions as discussed in Section 3.3.

In Table 1, all parameters of the various experiments performed are given. All in situ pictures shown here cover a surface area of $900 \times 900\,\mu m^2$. In all images, the growth direction is towards the top of the page.

Table 1
Parameters used in the Bridgman experiments

Figure	Material	Concentration (mass fraction in decane)	Translation velocity (μm/s)	Temperature hot finger/cold finger (°C)
2	SCN	1.00	7	90/50
3a	Tricosane	0.40	7	36/25
3b	Dotriacontane	0.75	7	85/25
4a	Tricosane	0.40	13	36/25
4b	Pentacosane	0.50	7	36/25
4c	Tricosane	0.40	13	36/25
4d	Tricosane	0.50	7	36/28
5a–c	Tricosane	0.50	7	36/25
6a	Dotriacontane	0.75	13	85/25
6b,b′	Tricosane	0.60	7	45/25
7a,b	Tricosane	0.75	7	36/25

3. Observations

3.1. Succinonitrile dendrites as a test case

Before addressing the complicated dendritic patterns of the paraffin crystals, some typical images of SCN dendrites grown from the melt are depicted in Fig. 2. As mentioned above, SCN, is a well-known model compound for the study of dendritic patterns [1]. Since it is a transparent organic compound with a melting temperature of 58°C, it is easy to study its solidification from an experimental point of view as compared to metals. Therefore, SCN is used frequently as a model compound in metallurgy. In Fig. 2, a steady growth front is advancing in the direction of the cold finger. In this case, the underlying lattice of SCN has a large angle with respect to the largest temperature gradient in the Bridgman furnace, which results in off-angle dendrites with larger side-arms in one direction. Close examination of the dendritic tips reveal the wavy patterns characteristic of the generation of side arms. Note that in Fig. 2, behind the growth front, recrystallization effects can be observed for the SCN dendrites. The space between adjacent side arms tends to disappear, resulting in one large elongated single crystal instead of the initial dendritic shape. This shape is energetically more favorable, since it results in less surface area. Holes can be observed, and result from the merging of side arms.

3.2. Tricosane, pentacosane and dotriacontane dendrites

In interpreting all in situ images of paraffin crystals presented in this paper, one must keep in mind that although they may appear two-dimensional, the crystals and their environment are three-dimensional. Further, for solution grown dendrites, an important difference as compared to melt grown crystals is that the relative amount of crystallizing material is much less, resulting in relatively more free space for a single dendrite to grow. In Fig. 3, typical tricosane and dotriacontane dendrites are shown. Note that the tips of both dendrites are comparable, but behind the growth front the recrystallization phenomena result in rather different shapes. In the case of the tricosane dendrites it is observed that the dendrites appear darker further back from the growth front, indicating a thin crystal close to the tip that gets thicker further away from the growth front (towards the cold finger). The same difference can be observed by comparing the darkness of the crystal areas near the edges and in the center. However, note that here the darker regions are at the edges, and are not the central areas. The recrystallization effects are very profound in the case of the tricosane dendrite, which reveals pinched-off arms and holes within the crystal. In addition, the different gray levels within the crystalline part of the images, which correlate with

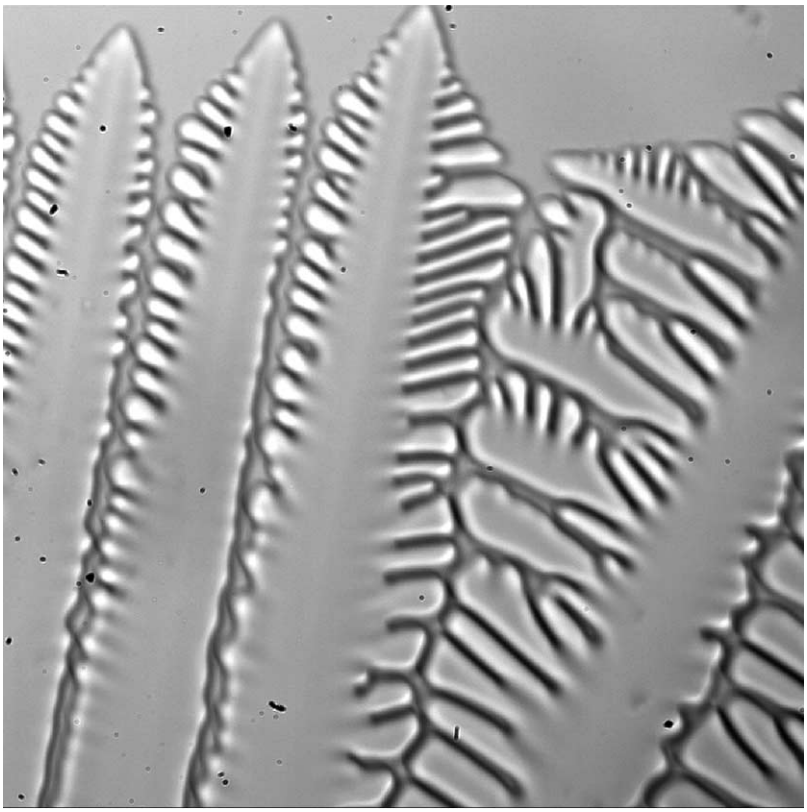

Fig. 2. Succinonitrile crystals showing the well-known dendritic patterns with side-arms growing out from the sinusoidal distortion of the parabolic front. Behind the growth front, recrystallization of the side-arms takes place.

the difference in crystal thickness, have a different source in these dendrites. For the dotriacontane dendrites (Fig. 3b) these are the result of different dendritic tips which are overlapping each other, whereas for the tricosane dendrites (Fig. 3a) the height differences are observed within a single dendritic arm, indicating growth or recrystallization of the dendrite itself. The image contrasts resulting from the locally increased thickness of the dendrite arms can easily be distinguished from edge diffraction effects, which are confined to a very narrow region, close to the resolution limit of the microscope objective used.

Different manifestations of recrystallization effects are depicted in more detail in Fig. 4. In Fig. 4a, it can be seen that if the velocity is increased for low fractions of tricosane, the dendritic shape exhibits many holes and recrystallization phenomena. This figure also shows that the recrystallization phenomena may manifest in different ways and that their course is not very well controlled. This can be seen by the absence of holes in the left dendrite, whereas holes occur irregularly in the right dendrite. More plate-like pinched off dendritic arms are generated for pentacosane dendrites as shown in Fig. 4b. In Fig. 4c, which was taken about one millimeter behind the growth front, the tricosane crystals exhibit darker and brighter regions indicating increasing thickness of the crystals. In Fig. 4d, the creation of a hole within the crystal surface can be seen, with darker regions indicating a thicker crystal around the edge of the hole. Sharp differences

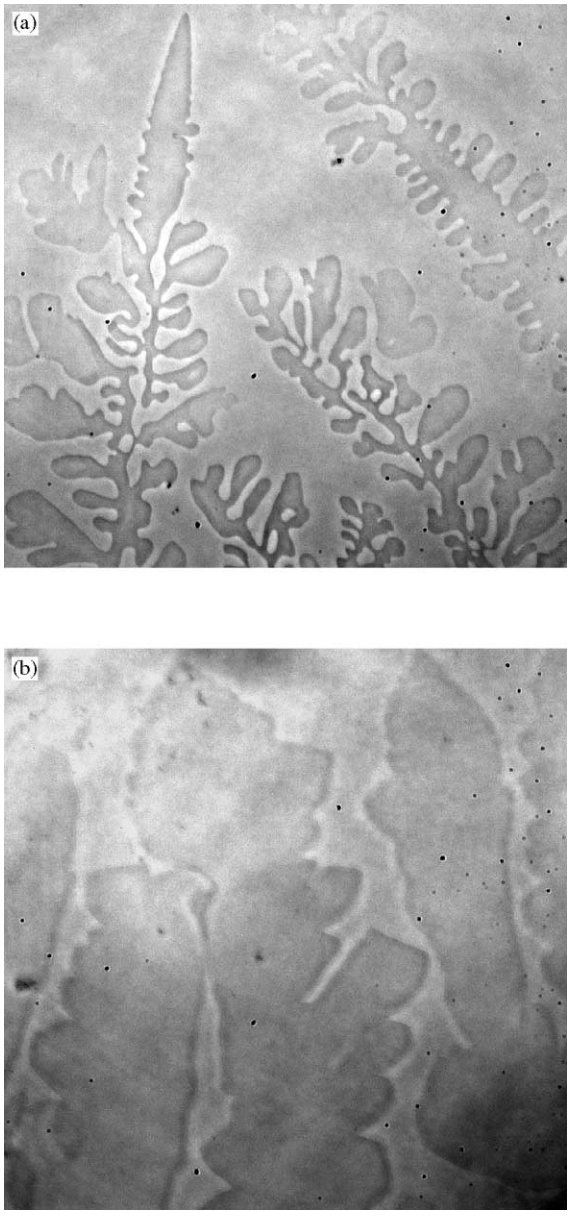

Fig. 3. (a) Tricosane dendrite showing recrystallization phenomena behind the dendritic tip, resulting in pinched off arms, increasing thickness and holes. (b) Dotriacontane dendrites showing only very thin crystals "sliding" over each other, but almost no recrystallization phenomena, result in locally increased gray levels.

in contrast can also be observed within the dendrites, indicating multiple steps, which imply that contrast differences within the crystals are not due to solid–solid state phase transition, but result from differences in crystal thickness.

Fig. 5 depicts three successive images of a growing tricosane dendrite. In these images the microscope was kept at a fixed position with respect to the dendritic coordinate frame by hand. In this way the effects of the recrystallization can be observed in time. Four important things can be seen from these images. First, the contrast of the interface increases from the tip to the base of the dendrite. The dendrite increases its width in time, indicating that lateral growth still proceeds after the first image is made. Second, at the rear of the dendrites the inner part of the dendrites appears much darker than at the tip, indicating thicker crystals. In Fig. 5b several different gray levels can be distinguished between the tip and the lower end of the dendrite. A close examination of Fig. 5c even shows more different levels of thickness within the main stem of the dendrite. Third, the width of the dendrite first increases, as in "traditional" melt grown dendrites, but where the darker regions appear it decreases again, contrary to the solidification model mentioned above. Fourth, several holes appear in the crystal, indicated by H_A and H_B in Fig. 5c. Only the occurrence of holes indicated with H_A are the results of merging side arms, similar to the SCN dendrites of Fig. 1. The holes indicated with H_B are formed spontaneously in the middle of the crystal, similar to those shown in Fig. 4d. Evidence for the "spontaneous" formation of holes in the dendrite crystals is given in Fig. 6. Fig. 6a shows a growing dotriacontane dendrite in which a number of holes are being formed at the central area of its surface. Figs. 6b and b′ are detailed images of a tricosane dendrite side arm before and after formation of the hole indicated by the arrow in Fig. 6b′.

3.3. Solid-solid phase transition

In Fig. 7 two successive images are shown that indicate the occurrence of a solid state phase transition of tricosane dendrites grown from a decane solution. In Fig. 7b, approximately 1 mm behind the growth front, a new front is observed showing a shift in gray level. The initially grown crystal surfaces seem to become roughened. The

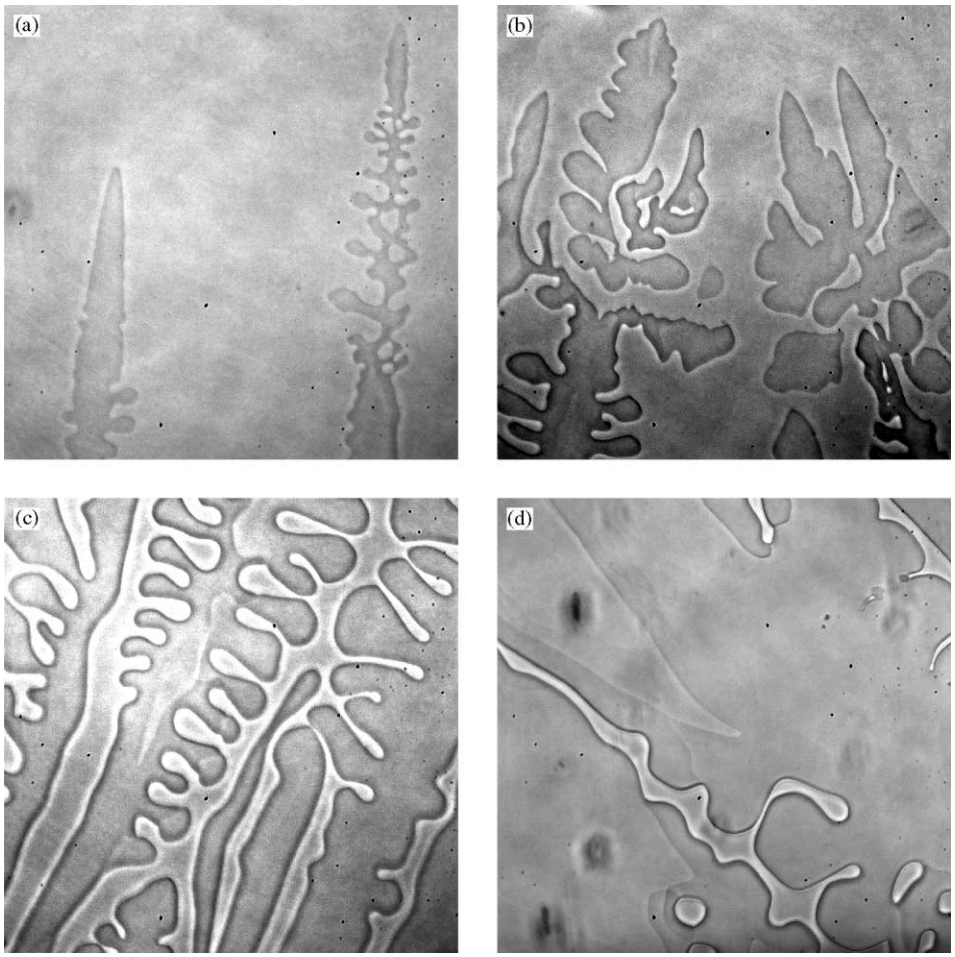

Fig. 4. Recrystallization phenomena of odd paraffins: (a) holes inside tricosane dendrites (b) pinching off of arms from pentacosane dendrites (c) thickening of the crystal by recrystallizing edges (d) combination of hole formation and thickening, indicated by the darker regions near the edges of the crystals. Multiple steps can be observed, showing that the contrasts do not present a solid–solid state phase transition.

transition, appearing as a moving interface parallel to the growth front, is only observed for highly concentrated solutions. In this example, the initial fraction of tricosane is 0.75. The solid state phase transition front propagates with the same velocity of 7 μm/s as the growth front. For the dendrites grown at lower fractions this phase transition was never observed clearly. Due to the deformation of the initially grown paraffin crystal surfaces, which can be seen by comparing the surfaces above and below the arrows indicated in Fig. 7b, the solid solid state transition front can be distinguished easily from thickening of the crystals as mentioned above. As in the experiments performed by Nozaki et al. [16–18] crack-like patterns appear that deform the initially grown surface morphology. They found that the transition front moves through a single pentacosane crystal reversibly when heating and cooling the crystal around the transition temperature of the low-ordered crystalline state and the rotator phase. In both cases, cracks appeared on the $\{0\,0\,1\}$ surface.

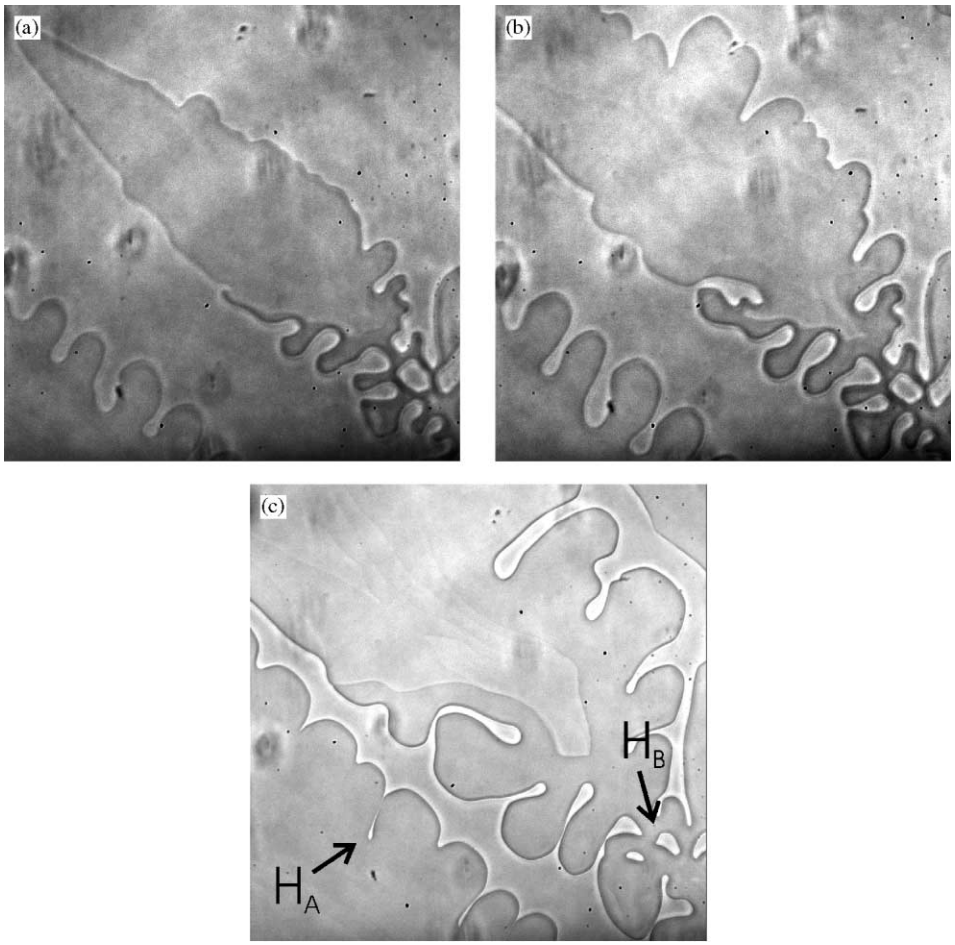

Fig. 5. Three successive images of a recrystallizing tricosane dendrite. The microscope is kept at a fixed position with respect to the dendrite coordinate system.

4. Two recrystallization mechanisms

The patterns appearing at the growth front of the SCN dendrites are characteristic dendritic patterns as predicted by solidification theory. Behind the growth front it can be observed that the morphology of the SCN dendrites changes due to further solidification and recrystallization, which leads to merging side arms. The patterns of the tricosane dendrites look different from the SCN dendrites, especially further away from the growth front: here recrystallization plays a major role. In this section two mechanisms are presented that may lead to this recrystallization. It is also shown that the pseudo two-dimensional structure of paraffins leads to a difference in growth patterns as compared to the SCN melt grown dendrites.

4.1. Surface minimization

From the simple Bravais–Friedel–Donnay–Harker theory (BFDH) [19,20], which predicts the morphological importance of a crystal face $(h\,k\,l)$ to be roughly inversely proportional to the interplanar thickness $d_{h\,k\,l}$, an approximate expression for the aspect ratio of paraffin crystals as a function of the number of carbon atoms can be

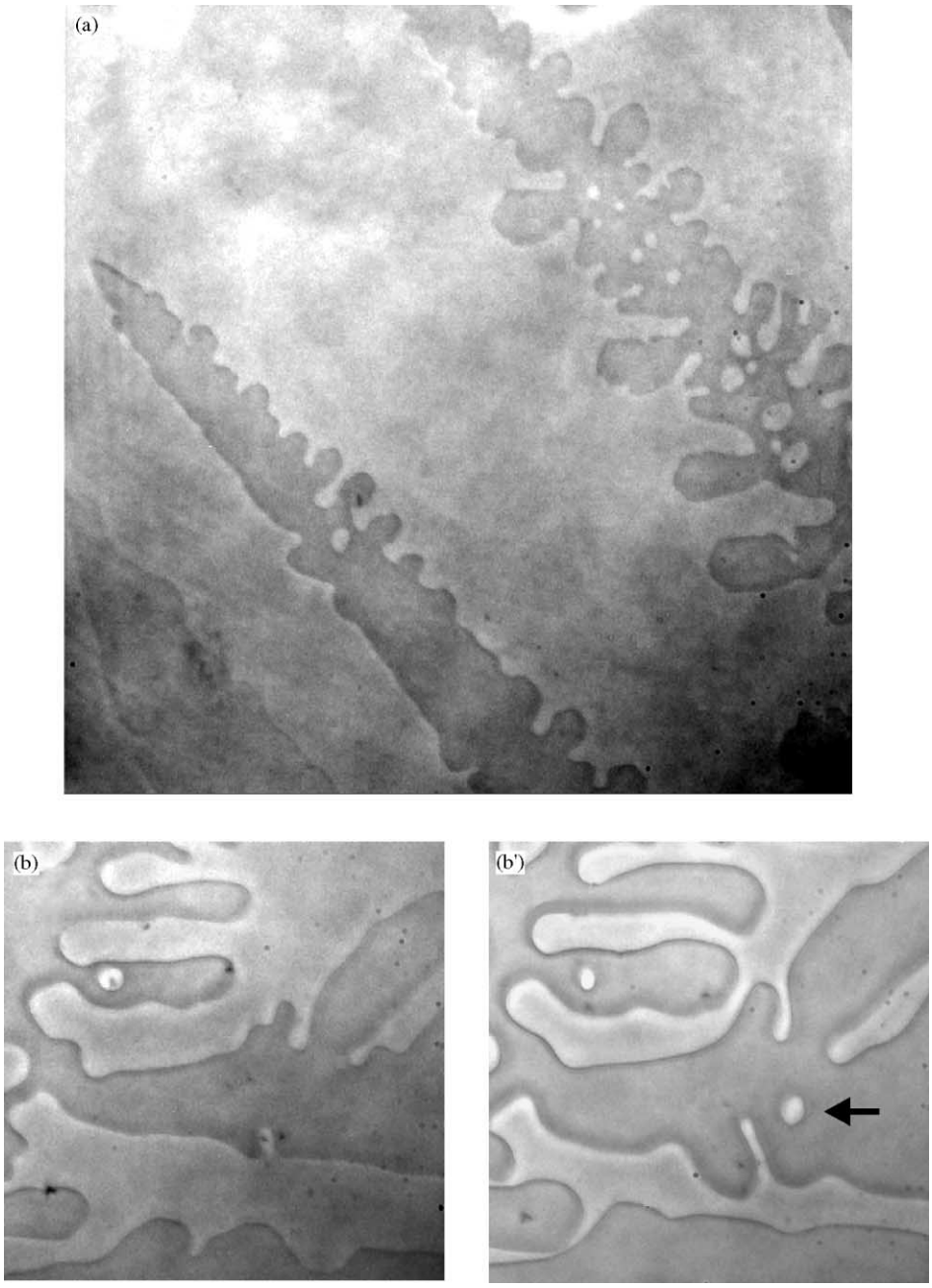

Fig. 6. Spontaneous development of holes in tricosane dendrites. (a) Growing dendrite with hole formation behind the tip. (b) and (b′) Dendrite side-arm before and after formation of a hole. The surface area of b and b′ is $450 \times 450\,\mu m^2$.

derived. Here we define the aspect ratio as the ratio of crystal width to its thickness. The lengths of the crystallographic axes are given by ($a = 7.42$ Å, $b = 4.96$ Å and $c = 2.54n + 3.693$ Å) and ($a = 4.96$ Å, $b = 7.478$ Å, $c = 2.546n + 3.75$ Å) for the even and odd numbered paraffins used,

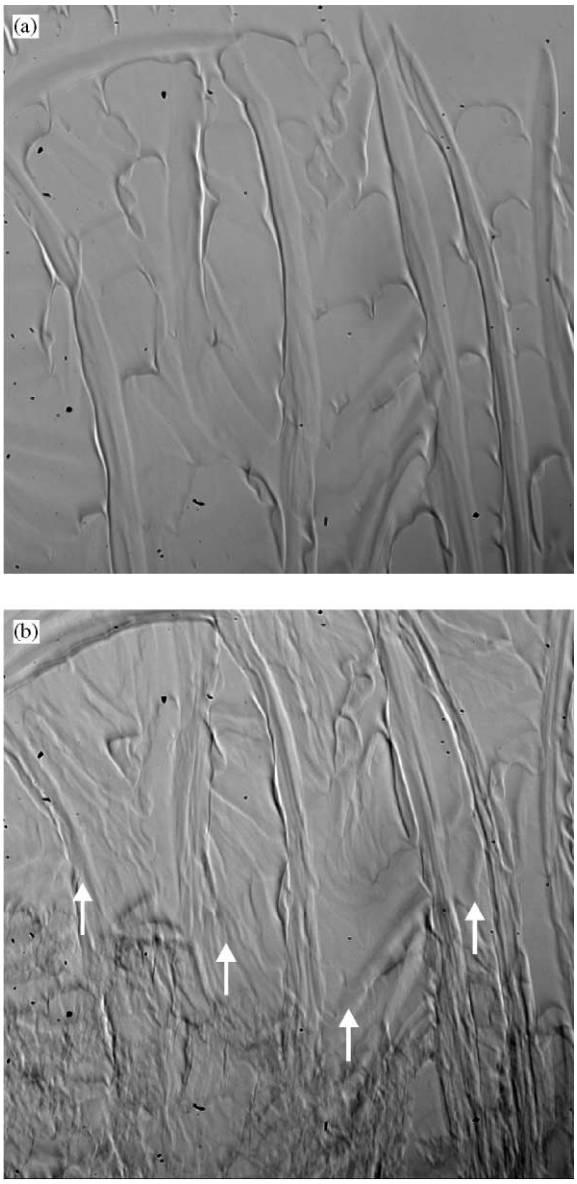

Fig. 7. Two successive images of tricosane dendrites grown from a 75 volume percent decane solution. Behind the growth front a new front can be seen that changes the surface morphology of the crystals, indicating the phase transition from the rotator phase to the orthorhombic phase.

respectively [21]. Hence, the aspect ratio A can be estimated by

$$A(n) \cong \frac{d_{0\,0\,2}}{\langle d_{\text{side}} \rangle} = \frac{c(n)}{(a+b)} \approx 0.4n + 0.6. \quad (1)$$

This simple formula indicates that the aspect ratios are: tricosane $A(23) \approx 9.8$, pentacosane $A(25) \approx 10.6$ and dotriacontane $A(32) \approx 13.4$. More sophisticated analysis, based on the Hartman–Perdok theory [11,22–25] results in better, but more complicated, estimates for the aspect ratios. For the growth form, based on the attachment energy, these studies predict aspect ratios of 10 for the growth form and 2 for the equilibrium form of tricosane [25]. Note that the effect of the number of carbon atoms is weak for all predicted morphologies. Boistelle [21] has pointed out that experimentally observed aspect ratios of n-alkanes are always larger than predicted values, because of the different growth mechanisms for both directions, i.e., spiral growth for $\{0\,0\,1\}$ faces and two-dimensional nucleation for the side faces.

The aspect ratios of the dendrite tips in our experiments are far off the estimated values, as suggested by Figs. 3 and 5. In our experiments, the imposed growth velocity is large. The different growth mechanisms of the top and the bottom faces (slow 2D nucleation or spiral growth) and the side faces (kinetically roughened growth leading to non-facetted shape) leads to larger aspect ratios [21]. Because the dendritic tips are barely visible in the optical microscope, their thickness is assumed to be 1 μm or somewhat less. This results in an aspect ratio at the tip of about 200 in Fig. 5a, which is about two orders of magnitude larger than the equilibrium value. In the same figure it can be seen that behind the tip, the width, i.e. the aspect ratio, decreases by approximately one order of magnitude.

The very large difference between the growth and equilibrium forms makes recrystallization very favorable, especially if this leads to thicker crystals. Consider Fig. 8, in which an initially disc-shaped crystal of radius R and thickness δ transforms into a thicker crystal of radius R' and thickness δ'. The proposed conversion mechanism is indicated by $A \rightarrow B \rightarrow C$. It is assumed that material is dissolving from the thin edges of the dendrite and recrystallizes on top of the $\{0\,0\,1\}$ faces near these edges. Assuming that the surface energy of a side face and that of the $\{0\,0\,1\}$ face are

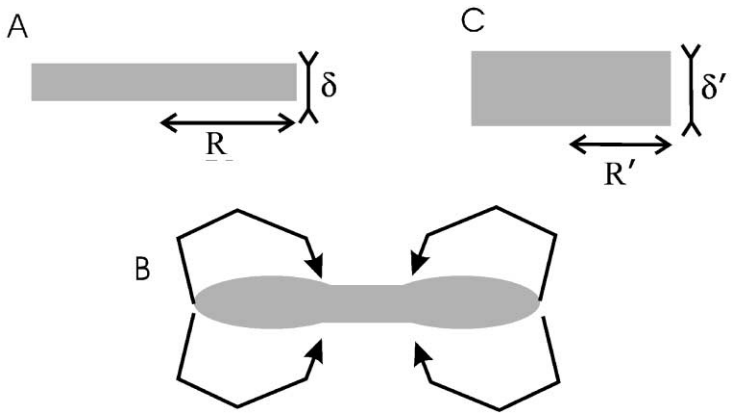

Fig. 8. Schematic drawing of recrystallization phenomena: material is dissolving from the edges of the crystals, and redeposited on top and bottoms of the {0 0 1} faces.

given by γ_{side} and $\gamma_{0\,0\,1}$, respectively, the difference in surface energy after recrystallization is given by

$$\Delta G = 2\pi((R')^2 - R^2)\gamma_{0\,0\,1} + 2\pi(R'\delta' - R\delta)\gamma_{\text{side}} \quad (2)$$

in which the crystal volume remains constant, i.e., $(R')^2\delta' = R^2\delta$.

This equation shows that recrystallization by increasing thickness is very efficient for extremely thin crystals like paraffins. Apart from increasing the crystal thickness, the surface area can also be minimized by reducing the surface perpendicular to the {0 0 1} face, i.e. the side faces, which make up the contour of the dendrites in all images. Although, increasing the thickness is kinetically more difficult because of a barrier for 2D nucleation or slow spiral growth, the gain in energy is very high, especially for longer n-alkanes. This increased thickness yields a larger energy gain than minimizing the perpendicular surface of the thin crystals. Therefore for the shorter n-alkanes, tricosane and pentacosane, thickness growth, even at the cost of increase of contour length, is the dominant process in recrystallization. It can be seen from Fig. 3b that there is no increase in thickness for the longer dotriacontane crystals, which can be explained by considering that two-dimensional nucleation growth on top of the {0 0 1} faces of these crystals is extremely slow. Moreover, in Fig. 5c, the shape of the hole resulting from two merging side arms, indicated with H_A, is very thin and elongated, implying that the curvature of the contour lines, i.e. the amount of side face area, is not that important.

4.2. Uptake and diffusion of solvent material

The mechanism mentioned above cannot explain the occurrence of holes that are observed to appear in the middle of many dendrites. The change of Gibbs free energy for the creation of a hole in a thin n-alkane crystal equals

$$\Delta G(r) = \Delta G_{\text{bulk}} + \Delta G_{\text{surface}} \quad (3)$$

or

$$\Delta G(r) = +\pi r^2\delta\Delta\mu - 2\pi r^2\gamma_{0\,0\,1} + 2\pi r\delta\gamma_{\text{side}}. \quad (4)$$

Here r is the radius of the hole, δ the crystal thickness and $\Delta\mu$ the driving force for growth. Assuming low supersaturation one obtains

$$\Delta G(r) = -2\pi r^2\gamma_{0\,0\,1} + 2\pi r\delta\gamma_{\text{side}}. \quad (5)$$

The critical radius r^* for a marginally stable hole can be found by solving this equation for $\partial\Delta G/\partial r = 0$, yielding an expression for r^* as

$$r^* = \frac{\delta\gamma_{\text{side}}}{2\gamma_{0\,0\,1}}. \quad (6)$$

This equation states that the critical radius must be of the order of the crystal thickness δ, assuming that surface energies are of the

same order. The activation barrier for forming a hole with this critical radius and its subsequent expansion is

$$\Delta G^* = \Delta G(r^*) = \frac{\pi\delta^2\gamma_{\text{side}}^2}{2\gamma_{0\,0\,1}}. \quad (7)$$

Taking $\delta \approx 1\,\mu\text{m}$ and $\gamma_{\text{side}} \approx \gamma_{0\,0\,1} = 30\,\text{m J m}^{-2}$ [14] one obtains $\Delta G^*/kT = 1.1\times10^7$, which is very large. It is obvious that the spontaneous formation of such large holes, having radii of the order of several hundred nanometers, can therefore be neglected. This suggests that such holes must be induced by a heterogeneous nucleation mechanism.

In Fig. 9 a reasonable mechanism is proposed for the creation of holes in the paraffin dendrites. Consider that during growth a certain amount of solvent material is incorporated in the crystal. Because the solvent is also an n-alkane, i.e., decane, and the crystallizing polymorph is most likely the rotator phase, solvent uptake is not very difficult. Moreover, because the rotator phase is hexagonal and lacks order in the $\{0\,0\,1\}$ plane, diffusion of decane solvent molecules within this plane is quite possible, leading to this segregation phenomenon. For the initially disc-shaped crystal depicted in Fig. 9, solvent molecules may diffuse in plane towards the edge or accumulate somewhere in the middle, leading to the generation of holes. Stress fields of dislocations perpendicular to the $\{0\,0\,1\}$ planes may enhance this process. Once such a hole exceeds its critical radius r^*, then it will expand by recrystallization as mentioned above.

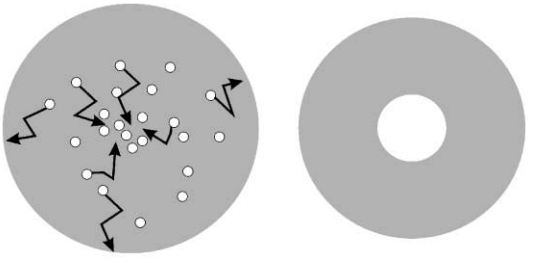

Fig. 9. Solvent diffusion within the tricosane dendrites: some of the solvent molecules diffuse to the edges; the rest diffuses towards each other, creating stable holes.

5. Conclusion

It is shown that paraffin dendrites can be grown from solution using our in situ Bridgman furnace. However, to explain the morphological features observed, additional factors have to be considered, making the analysis of these crystals more complex than that of "traditionally" melt-grown dendrites, such as SCN.

The anomalous shapes of the paraffin dendrites observed are explained by considering that the morphologically unstable patterns tend to minimize their excess of surface energy after growth, as observed in tricosane and pentacosane. The most effective way to minimize the surface free energy of these extremely thin crystals is by increasing their thickness. However, for the longer chain paraffin, dotriacontane, this post-growth recrystallization is not observed, because of a large 2D-nucleation barrier for thickness growth. The formation of holes in the dendrites is explained by post-growth transport and subsequent segregation of decane as an impurity in the crystals, i.e. sweating out of solvent material. All of these observed anomalous shapes could also be regarded as transition shapes of an aging process of freshly grown dendrites that appears on very small time scale.

Acknowledgements

R.L.A. Roersch and A.P.G. Steegs (HTS Venlo, the Netherlands) and J. Nieboer (Technical department of the University of Nijmegen) are acknowledged for the development and construction of the in situ Bridgman furnace, respectively. Dr. C.C. Perry of the Nottingham Trent University is acknowledged for making the stay of O. Stasse at the Solid State Department of the University of Nijmegen possible. Finally, the authors whish to thank the referee for his valuable comments that improved this paper.

References

[1] M.E. Glicksman, S.P. Marsh, in: D. Hurle (Ed.), Handbook of Crystal Growth, Elsevier, Amsterdam, 1993, p. 1075.

[2] K. Kassner, in: J.P. van der Eerden, O.S.L. Bruinsma (Eds.), Science and Technology of Crystal Growth, Kluwer Academic Publishers, Dordrecht, 1995, p. 193.
[3] D. Meiron, Phys. Rev. A. 33 (1984) 2704.
[4] H. Müller-Krumbhaar, in: I. Sunagawa (Ed.), Morphology of crystals—Part B, Terra Scientific Publishing Company (TERRAPUB), Tokyo, 1987, p. 613.
[5] R. Kobayashi, J.A. Warren, W.C. Carter, Physica D 119 (1998) 415.
[6] D.D. Saratovkin, Dendritic Crystallization, Chapman & Hall, London, 1959.
[7] M. Bienfait, R. Kern, Bull. Soc. Fr. Mineral. Cristallogr. 87 (1964) 604.
[8] M.G. Broadhurst, J. Res. Natural Bur. Stand. Section A 66 (1962) 241.
[9] L.A.K. Stavely, Quart. Rev. (London) 3 (1949) 65.
[10] R.T. Turner, Ind. Eng. Chem. Prod. Res. Dev. 10 (1971) 238.
[11] P.J.C.M. van Hoof, R.F.P. Grimbergen, H. Meekes, W.J.P. van Enckevort, P. Bennema, J. Crystal Growth 191 (1998) 861.
[12] E.B. Sirota, H.E. King Jr., D.M. Singer, H.H. Shao, J. Chem. Phys. 98 (1993) 5809.
[13] P. Bennema, in: D. Hurle (Ed.), Handbook of Crystal Growth, Elsevier, Amsterdam, 1993, p. 563.
[14] P.J.C.M. van Hoof, W.J.P. van Enckevort, M. Schoutsen, J. Crystal Growth 183 (1998) 679.
[15] P.J.C.M. van Hoof, W.J.P. van Enckevort, M. Schoutsen, P. Bennema, X.Y. Liu, J. Crystal Growth 183 (1998) 109.
[16] K. Nozaki, N. Higashitani, T. Yamamoto, T. Hira, J. Chem. Phys. 103 (1995) 5762.
[17] K. Nozaki, T. Yamayoto, T. Hara, M. Hikosaka, Jpn. J. Appl. Phys. 36 (1997) L146–L49.
[18] K. Nozaki, M. Hikosaka, Jpn. J. Appl. Phys. 37 (1998) 3450.
[19] G. Friedel, Bull. Soc. Fr. Mineral. Cristallogr. 30 (1907) 326.
[20] J.D.H. Donnay, D. Harker, Am. Mineralogist 22 (1937) 446.
[21] R. Boistelle, in: E. Kaldis (Ed.), Current topics in materials science, Elsevier, North-Holland, 1980, p. 413.
[22] X.Y. Liu, P. Bennema, J. Chem. Phys. 98 (1993) 5863.
[23] X.Y. Liu, P. Bennema, J. Appl. Crystallogr. 26 (1993) 229.
[24] X.Y. Liu, P. Bennema, J. Crystal Growth 135 (1994) 209.
[25] R.F.P. Grimbergen, P.J.C.M. van Hoof, H. Meekes, P. Bennema, J. Crystal Growth 191 (1998) 846.